Article

Rate of mass loss from the Greenland Ice Sheet will exceed Holocene values this century

https://doi.org/10.1038/s41586-020-2742-6

Received: 30 December 2019

Accepted: 27 July 2020

Published online: 30 September 2020

Check for updates

Jason P. Briner[1]✉, Joshua K. Cuzzone[2,3], Jessica A. Badgeley[4], Nicolás E. Young[5], Eric J. Steig[4,6], Mathieu Morlighem[2], Nicole-Jeanne Schlegel[3], Gregory J. Hakim[6], Joerg M. Schaefer[5,7], Jesse V. Johnson[8], Alia J. Lesnek[1], Elizabeth K. Thomas[1], Estelle Allan[9], Ole Bennike[10], Allison A. Cluett[1], Beata Csatho[1], Anne de Vernal[9], Jacob Downs[8], Eric Larour[3] & Sophie Nowicki[11]

The Greenland Ice Sheet (GIS) is losing mass at a high rate[1]. Given the short-term nature of the observational record, it is difficult to assess the historical importance of this mass-loss trend. Unlike records of greenhouse gas concentrations and global temperature, in which observations have been merged with palaeoclimate datasets, there are no comparably long records for rates of GIS mass change. Here we reveal unprecedented mass loss from the GIS this century, by placing contemporary and future rates of GIS mass loss within the context of the natural variability over the past 12,000 years. We force a high-resolution ice-sheet model with an ensemble of climate histories constrained by ice-core data[2]. Our simulation domain covers southwestern Greenland, the mass change of which is dominated by surface mass balance. The results agree favourably with an independent chronology of the history of the GIS margin[3,4]. The largest pre-industrial rates of mass loss (up to 6,000 billion tonnes per century) occurred in the early Holocene, and were similar to the contemporary (AD 2000–2018) rate of around 6,100 billion tonnes per century[5]. Simulations of future mass loss from southwestern GIS, based on Representative Concentration Pathway (RCP) scenarios corresponding to low (RCP2.6) and high (RCP8.5) greenhouse gas concentration trajectories[6], predict mass loss of between 8,800 and 35,900 billion tonnes over the twenty-first century. These rates of GIS mass loss exceed the maximum rates over the past 12,000 years. Because rates of mass loss from the southwestern GIS scale linearly[5] with the GIS as a whole, our results indicate, with high confidence, that the rate of mass loss from the GIS will exceed Holocene rates this century.

The GIS lies within the rapidly warming Arctic, and its contribution to sea-level rise has recently accelerated[1]. The increased rate of GIS mass loss since the 1990s is substantial, but the lack of data on long-term GIS mass change makes it difficult to evaluate this short-term phenomenon within the context of natural variability[5,7]. Efforts to quantify rates of ice-mass loss through time have relied on historical climate data and image analysis, contemporary airborne and satellite observations, and numerical ice-sheet simulations[5,8,9]. Combined, these approaches reveal that the GIS was roughly in neutral mass balance during the nineteenth century, experienced variable mass loss in the twentieth century, and has undergone a substantial increase in mass loss in the past 20 years[1,5,10]. The future of GIS mass change is uncertain, but projected warming combined with feedbacks in the coupled ice-sheet–climate system will lead to continued losses[9,11,12]. Given plausible future climate scenarios, the GIS may be entirely gone in as few as 1,000 years[13].

The GIS's past

Continuous time series of GIS mass change spanning centuries or longer are required to place the contemporary increase in mass loss in a longer-term context and to improve knowledge of the overall response of the GIS to climate change. Assembling such time series is challenging, owing to the reliance on numerical ice-sheet simulations that require climate boundary conditions from before the instrumental era. Ice-sheet reconstructions during warmer-than-present periods (for example, the early Holocene) are particularly relevant for modelling future ice-sheet changes.

Geological observations of GIS change are most abundant during the Holocene[14]. For this reason, the Holocene has been targeted as a timeframe for simulating GIS history[15–20]. Model simulations so far have been used to assess spatiotemporal patterns of GIS retreat and to constrain its minimum size. Simulated changes in ice volume are largely the product of climatic forcing; palaeo-mass balance is typically modelled using one of

[1]Department of Geology, University at Buffalo, Buffalo, NY, USA. [2]Department of Earth System Science, University of California Irvine, Irvine, CA, USA. [3]Jet Propulsion Laboratory, California Institute of Technology, Pasadena, CA, USA. [4]Department of Earth and Space Sciences, University of Washington, Seattle, WA, USA. [5]Lamont-Doherty Earth Observatory, Geochemistry, Palisades, NY, USA. [6]Department of Atmospheric Sciences, University of Washington, Seattle, WA, USA. [7]Department of Earth and Environmental Sciences, Columbia University, New York, NY, USA. [8]Department of Computer Science, University of Montana, Missoula, MT, USA. [9]Geotop, Université du Québec à Montréal, Montréal, Quebec, Canada. [10]Geological Survey of Denmark and Greenland, Copenhagen, Denmark. [11]Cryospheric Sciences Laboratory, Goddard Space Flight Center, NASA, Greenbelt, MD, USA. ✉e-mail: jbriner@buffalo.edu

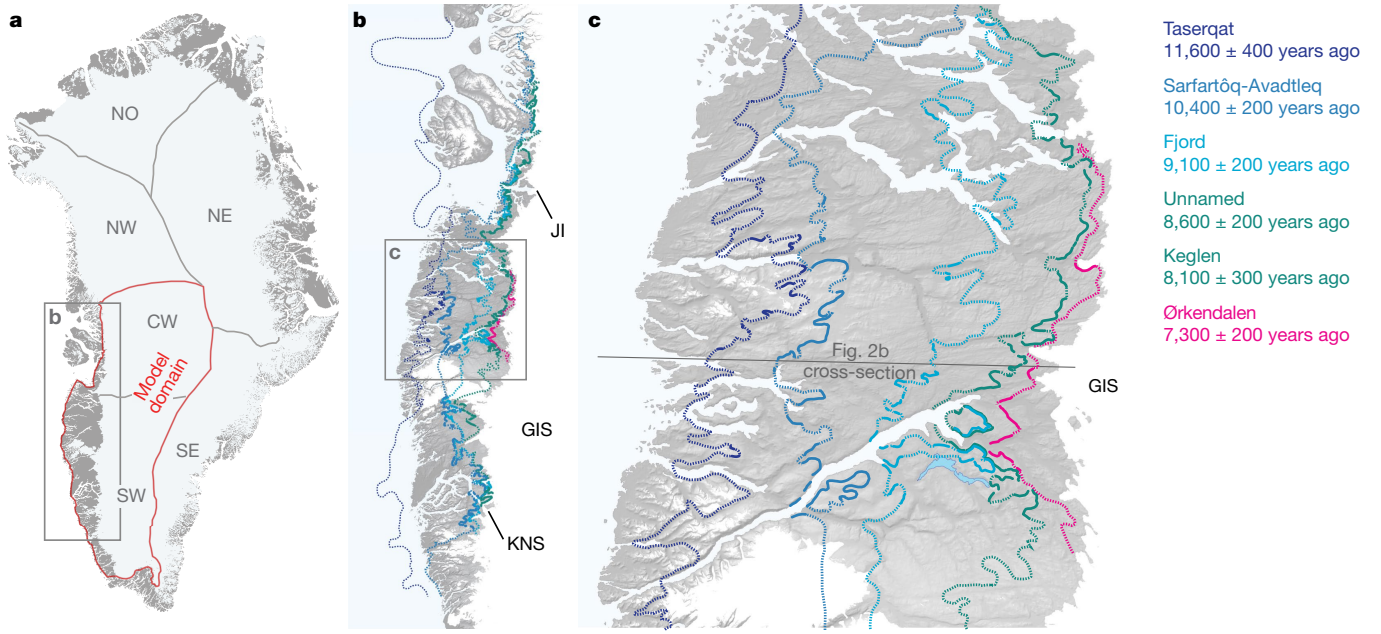

Fig. 1 | Domain for the ice-sheet model and moraine record of past GIS change in SW Greenland. a, Map of the present-day GIS, showing commonly used domains (as labelled) and our model domain (outlined in red). NO, north; NE, northeast; NW, northwest; CW, central-west; SE, southeast; SW, southwest. **b**, WSW Greenland (boxed in **a**), showing widely traceable moraine sequences[3]. JI, Jakobshavn Isbræ; KNS, Kangiata Nunaata Sermia. **c**, Cosmogenic-nuclide exposure-age chronologies of all moraines between the ocean and the GIS[4] (boxed in **b**); 1σ age uncertainties are listed; moraine lines are dashed where uncertain. Base-map topography from BedMachine[37].

the ice-core $\delta^{18}O$ time series from central Greenland, which is converted to temperature and precipitation, and scaled across the ice sheet[15]. Some approaches improve model performance with geological constraints, but climate forcing is still scaled from limited ice-core data, sometimes using prescribed Holocene temperature histories to improve model–data fit[16,17]. One recent study[19] used data averaged from three ice-core sites to adjust palaeotemperatures from a transient climate model, and scaled precipitation from one ice-core accumulation record. All these estimates of mass-loss rates during the Holocene provide important context for projected GIS mass loss, but they have not been extended into the future, making quantitative comparisons uncertain.

GIS modelling

We place today's rates of ice loss into the context of the Holocene and the future using a consistent framework, by simulating rates of GIS mass change from 12,000 years ago to AD 2100. We use the high-resolution Ice Sheet and Sea-level system Model (ISSM), which resolves topography as finely as 2 km (refs. [21–23]). Our simulations are forced with a palaeoclimate reanalysis product for Greenland temperature and precipitation over the past 20,000 years[2]. This reanalysis was derived using data assimilation of Arctic ice-core records (oxygen isotopes of ice, and snow accumulation) with a transient climate model (Methods). We account for uncertainty in the temperature and precipitation reconstructions by creating an ensemble of nine individual ISSM simulations that have varying temperature and precipitation forcings[2] (Methods). Sensitivity tests using a simplified model in the same domain[24] suggest that the range in plausible palaeoclimate forcing, which we use, has a larger influence on simulated rates of ice-mass change than do model parameters such as basal drag, surface-mass-balance parameters and initial state. We compare our simulated GIS extent against mapped and dated changes in the position of the GIS margin[3,4].

Much of the GIS perimeter is dominated by marine-terminating glaciers with calving dynamics that are challenging to simulate, particularly on long timescales[25]. We focus on a regional model domain covering the southwest and central-west drainage basins of the GIS[26] (collectively referred to as the west–southwest, WSW), with the domain extending outward to the present-day coastline (Fig. 1). Despite including the dynamically complex Jakobshavn Isbræ basin, our domain is dominated by Greenland's largest tract of land-based ice and thus has relatively little direct marine coupling. Glacier variations in WSW Greenland are dominated by surface mass balance, simplifying the model requirements. Most other sectors of the GIS are more strongly influenced by marine-terminus ice dynamics, which are difficult to simulate accurately[23,26,27]. Nevertheless, observations since 1972 reveal a tight agreement between the rate of mass change in our model domain and the entire GIS[5]. Hence, our region can be considered representative of the GIS as a whole. Furthermore, the Holocene glacier history in this region is well constrained[3,4], providing independent validation of our model results.

12,000 years of natural variability

Our simulations are divided into three experiments (Methods): Holocene (12,000 years ago to AD 1850), historic (AD 1850–2012) and future (AD 2015–2100). Our Holocene simulations show eastward ice retreat throughout our domain between approximately 12,000 and 7,000 years ago, after which the ice sheet shows relatively small ice-margin changes (Fig. 2, Methods). Our simulated pattern of WSW GIS size through the Holocene is consistent with three lines of evidence from glacial–geologic reconstructions[3,28]. First, widely traceable moraine systems in WSW Greenland delimit GIS recession between 12,000 and 7,000 years ago[3,4,29]. Our simulated ice-margin locations closely resemble the independent evidence of ice-margin history. In the portion of our domain with the richest moraine record, the simulated ice area is −20% to +4% the size of the ice area constrained by observations (that is, moraines; Fig. 2, Methods). In some sectors, particularly at Jakobshavn Isbræ and near Kangia Nunata Sermia (Fig. 1), simulated ice-margin recession occurs later than observations suggest (Methods). In addition, the simulated present ice margin is more extensive than the present ice extent along the southern portion of our model domain (local precipitation anomalies could help to explain some of the offset[24]), but there is agreement with the present ice margin throughout most of our domain (Methods). Second, the prominent

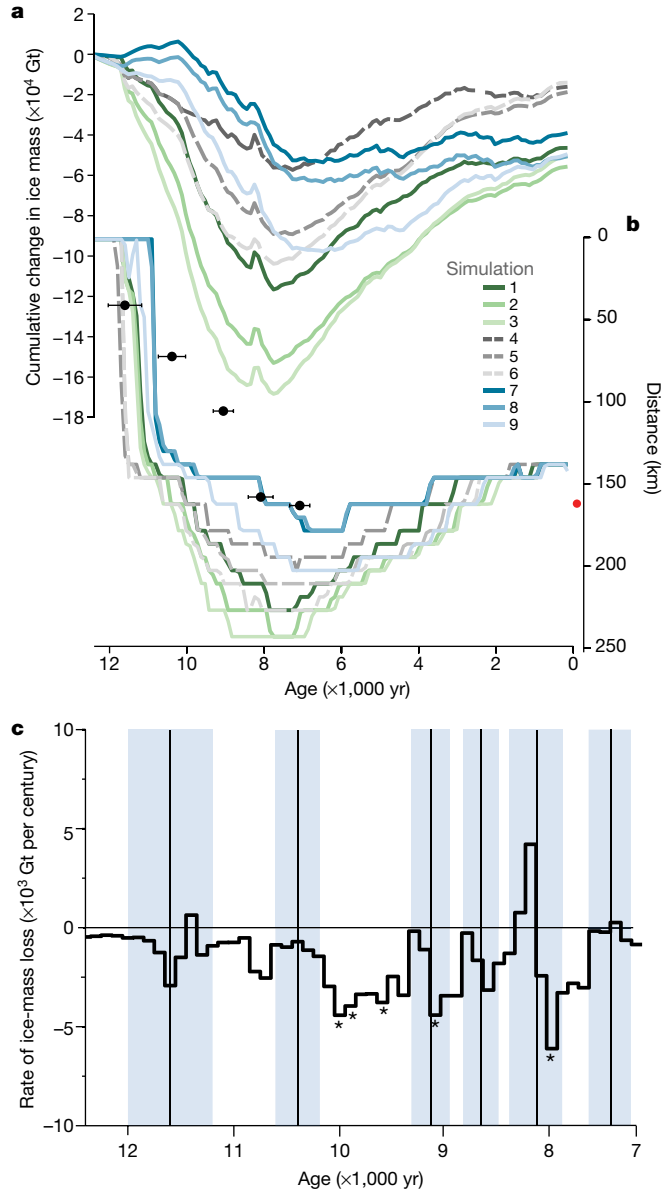

Fig. 2 | Increased and variable GIS mass loss during the Holocene. **a**, Simulated cumulative change in WSW GIS ice mass from 12,000 years ago to AD 1850, for nine model simulations (Methods). **b**, Simulated position of the WSW GIS margin in the Holocene, for the transect shown in Fig. 1c. Black circles represent independent observations of ice-margin position based on mapped and dated moraines (with one-standard-deviation age uncertainty); the red circle is the present-day GIS margin. **c**, Bar plot showing the mean rate of ice-mass loss from 12,500 to 7,000 years ago; vertical lines and shading show moraine age and one-standard-deviation uncertainty for every moraine between Baffin Bay and the present-day ice margin[4]; asterisks mark the five centuries with the highest rates of mass loss.

moraine belts in our domain represent widespread still-stands (that is, minimal rate of ice-mass change) and/or re-advances (that is, ice-mass gain) during the early and middle Holocene[4], providing an additional means of comparison with our simulation. Our simulated GIS mass change approaches neutral or becomes positive at 11,400, 10,400, 9,200, 8,600, 8,200 and 7,300 years ago (Fig. 2); each of these periods corresponds to a time of moraine deposition, which requires neutral or positive GIS mass change[4]. Similarly, there are no moraines dating to the multi-centennial intervals during which our simulations show increased mass loss, such as from 10,400 to 9,200 years ago (Fig. 2). Third, sedimentary evidence reveals greatly reduced ice-margin recession beginning around 7,000 years ago, slightly smaller-than-present ice extent around 6,000 to 4,000 years ago, and a late Holocene ice-margin position close to the present-day one[3]. These patterns of relatively minor ice-sheet changes after 7,000 years ago are also consistent with our simulated WSW GIS history (Supplement Videos 1 and 2). The overall agreement between the simulated and reconstructed history of the WSW GIS margin lends confidence to our simulated rates of early-Holocene ice-mass change.

Mass loss between 10,000 and 7,000 years ago exceeded rates of loss during any other time in the Holocene (Fig. 3), ranging from positive (during brief cold-climate events) to multi-century intervals with rates of ice-mass loss of up to 6,000 Gt per century (ensemble-mean value). The five centuries with the highest mass-loss values average 4,900 ± 1,400 Gt per century (Fig. 2; ensemble-mean values and two-standard-deviation uncertainty). The timing and duration of higher-than-average early-Holocene mass loss is consistent with most palaeoclimate and glacial geologic records from the Arctic, which reveal a well-documented thermal maximum in the early Holocene that was 3 ± 1 °C warmer than the pre-industrial period[18,30–32]. Increased

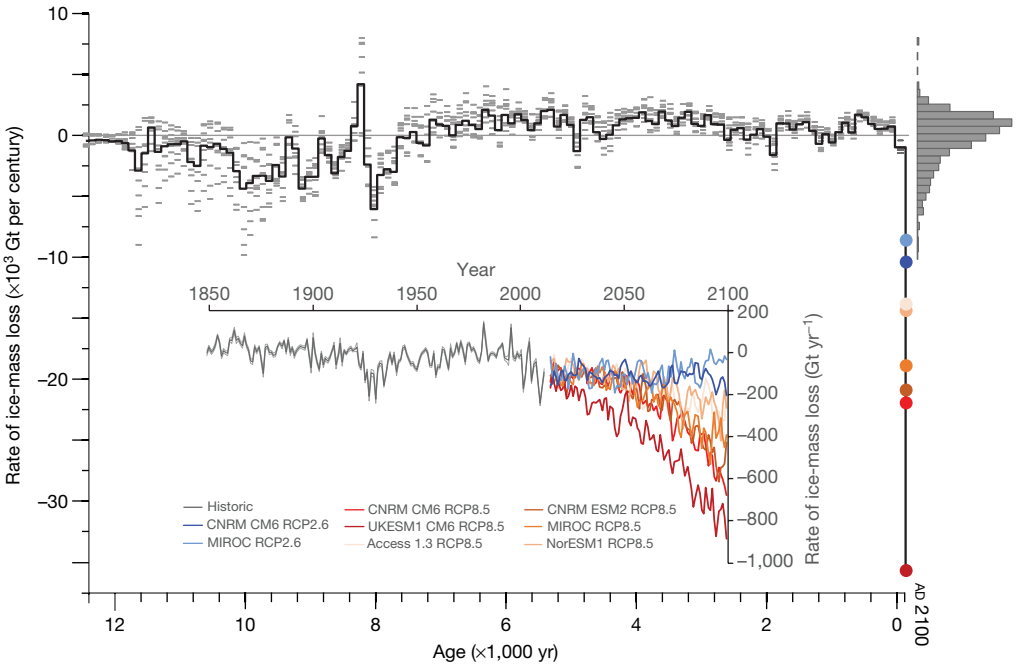

Fig. 3 | Exceptional rates of ice-mass loss in the twenty-first century, relative to the Holocene. The mean rate of ice-mass change each century, from 12,500 years ago to AD 2100, is shown by the black line. The light grey bars indicate the ice-mass change in each of the nine simulations. For the 1900s, simulated rates are shown in dark grey. For the 2000s, rates of ice-mass change for various RCP2.6 and RCP8.5 simulations are shown as blue and red circles (see legend in inset). The histogram on the right incorporates all (n = 1,125) Holocene rates of ice-mass change. The inset shows simulated rates of ice-mass change in annual timesteps from AD 1850 to AD 2100.

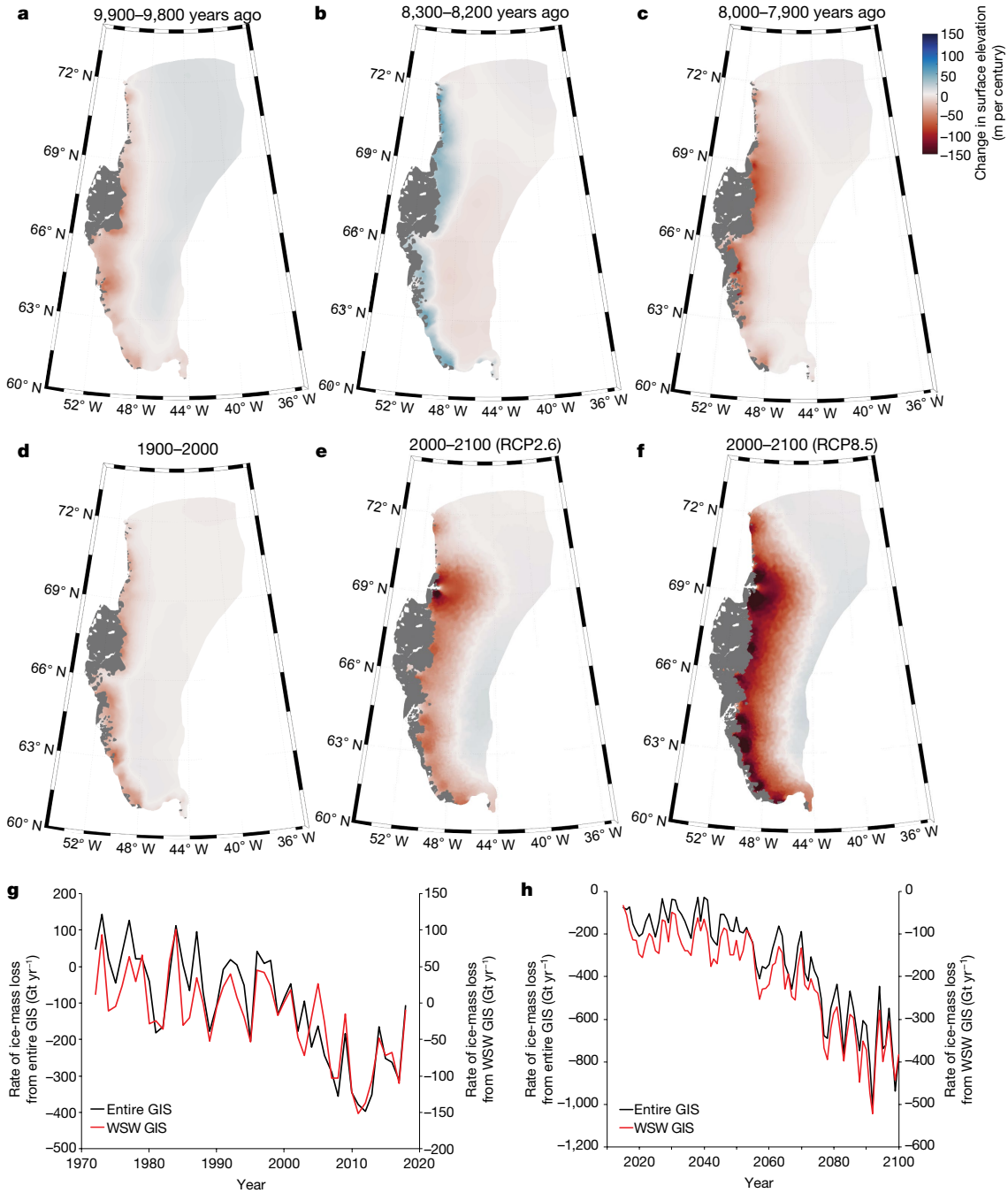

Fig. 4 | Substantial change in surface elevation of the GIS over the twenty-first century. a–**c**, Simulated change in surface elevation of WSW GIS (metres per century; colour scale) for the centuries in the Holocene with the highest mass-loss rate (**a**, **c**) and during the cold event 8,200 years ago (**b**), from model experiment 9. **d**–**f**, Simulated change in surface elevation (metres per century; colour scale) over the twenty-first century under the MIROC RCP2.6 (**e**) and RCP8.5 (**f**) scenarios, compared to the twentieth century (**d**). **g**, Comparison of the mass-loss rate for WSW GIS (right axis, red) and for the entire GIS (left axis, black), from AD 1972 to AD 2018, based on observations[5] ($r^2 = 0.82$, where r is the correlation coefficient). **h**, Comparison of the mass-loss rate for WSW GIS (right axis, red) and for the entire GIS (left axis, black), from AD 2015 to AD 2100, from our simulation using the MIROC RCP8.5 climate forcing ($r^2 = 0.97$).

ice-mass loss in the early Holocene is also consistent with surface ocean records around southern Greenland, indicating greatly reduced salinity, owing to meltwater discharge until about 7,000 years ago[33,34]. In addition, our simulated rates of mass loss from WSW GIS in the early Holocene are comparable to findings from other recent model experiments[19,20], providing further confidence that our simulations capture the range of ice-mass loss under natural variability during the Holocene. The maximum rates of ice-mass loss in the Holocene exceed our simulated rates of ice-mass loss in the historic interval (AD 1900–2000) of around 1,600 Gt per century (Methods), which is similar to an independent AD 1900–2000 estimate of 1,700 Gt per century for WSW GIS[8].

Historic and future ice-mass change

The substantial increase in rates of GIS mass loss in the past two decades is exceptional in the context of estimates of mass loss in the historic interval[5,8,9,35]. If the rates of mass loss observed over the past two decades were to remain constant for the rest of the twenty-first century, the total rate of mass loss over the twenty-first-century would be around 6,100 Gt

per century for WSW Greenland[5]. This value is within the low end of our simulated range of mass-loss rates during the early Holocene. However, 6,100 Gt per century may vastly underestimate the rate of mass loss for the twenty-first century, because climate is projected to become increasingly unfavourable for maintaining even the current levels of GIS mass balance[6]. Our simulations of twenty-first-century WSW GIS mass loss, using an identical model and model set-up, address the limitation of extrapolating observed rates of mass loss and yield century-average mass-loss rates of 8,800–10,600 Gt per century for RCP2.6 scenarios and 14,000–35,900 Gt per century for RCP8.5 scenarios (Methods, Fig. 3). Rates of GIS mass loss become less negative by AD 2100 in the simulations using RCP2.6 scenarios, consistent with recent results that show that the GIS remains sizeable into the future under low-carbon-emission scenarios[13]. By contrast, the marked and increasing GIS mass loss in the simulations using RCP8.5 scenarios is consistent with recent findings that Greenland could become ice-sheet-free in as few as 1,000 years[13]. Because the rate of ice-mass change in WSW Greenland mirrors that of the entire GIS (Fig. 4, Methods), our findings probably represent the pattern of ice-mass loss for the entire GIS. In addition, simulations of future GIS evolution show an increasing influence of surface mass balance[13,36], further supporting the representativeness of our model domain.

Our simulated rates of mass loss from WSW GIS for this century (8,800–35,900 Gt per century, or 2.4–9.9 cm sea-level equivalent) exceed our simulated Holocene mass-loss rates (Fig. 3). Among all available twenty-first-century simulations, only one of the two RCP2.6 runs (MIROC, −8,800 Gt per century) falls within the range of our Holocene simulations at the 99th percentile; all others lie outside the 99th percentile. The recent observed trend in GIS mass loss is following the RCP8.5 trajectory[1], which suggests that ongoing mass loss this century is likely to be represented among our simulated RCP8.5 rates. If so, the amount of ice loss in WSW Greenland this century would reverse the previous 4,000 years of cumulative ice growth and exceed maximum Holocene mass-loss rates by a factor of about four. Comparison with a recent GIS model intercomparison effort to assess ice-mass loss up to AD 2100 shows that our simulations are at the low end of the model spread[36]. Thus, our simulated future rates of change in billions of tonnes per century are relatively conservative. These findings could change when using fully coupled ice-sheet–climate models; however, feedbacks that become apparent in coupled simulations[9] should affect the past and future similarly. Therefore, we do not expect the pattern of rate of ice-mass loss over time to differ substantially. Our results suggest that the rate of mass loss from the GIS this century will be unprecedented in the context of natural GIS variability over the past 12,000 years, unless a low-carbon-emission scenario is followed. This provides further evidence that low carbon emissions are critical to mitigate contributions of the GIS to sea-level rise.

Online content

Any methods, additional references, Nature Research reporting summaries, source data, extended data, supplementary information, acknowledgements, peer review information; details of author contributions and competing interests; and statements of data and code availability are available at https://doi.org/10.1038/s41586-020-2742-6.

1. The IMBIE Team. Mass balance of the Greenland Ice Sheet from 1992 to 2018. *Nature* **579**, 233–239 (2020).
2. Badgeley, J. A., Steig, E. J., Hakim, G. J. & Fudge, T. J. Greenland temperature and precipitation over the last 20,000 years using data assimilation. *Clim. Past* **16**, 1325–1346 (2020).
3. Lesnek, A. J., Briner, J. P., Young, N. E. & Cuzzone, J. K. Maximum southwest Greenland Ice Sheet recession in the early Holocene. *Geophys. Res. Lett.* **47**, e2019GL083164 (2020).
4. Young, N. E. et al. Deglaciation of the Greenland and Laurentide ice sheets interrupted by glacier advance during abrupt coolings. *Quat. Sci. Rev.* **229**, 106091 (2020).
5. Mouginot, J. et al. Forty-six years of Greenland Ice Sheet mass balance from 1972 to 2018. *Proc. Natl Acad. Sci. USA* **116**, 9239–9244 (2019).
6. Pörtner, H.-O. et al. (eds) *IPCC Special Report on the Ocean and Cryosphere in a Changing Climate* Ch. 3 (2019); https://www.ipcc.ch/srocc/
7. Bevis, M. et al. Accelerating changes in ice mass within Greenland, and the ice sheet's sensitivity to atmospheric forcing. *Proc. Natl Acad. Sci. USA* **116**, 1934–1939 (2019).
8. Kjeldsen, K. K. et al. Spatial and temporal distribution of mass loss from the Greenland Ice Sheet since AD 1900. *Nature* **528**, 396–400 (2015).
9. Golledge, N. R. et al. Global environmental consequences of twenty-first-century ice-sheet melt. *Nature* **566**, 65–72 (2019).
10. Box, J. E. & Colgan, W. Greenland Ice Sheet mass balance reconstruction. Part III: marine ice loss and total mass balance (1840–2010). *J. Clim.* **26**, 6990–7002 (2013).
11. Robinson, A., Calov, R. & Ganopolski, A. Multistability and critical thresholds of the Greenland ice sheet. *Nat. Clim. Chang.* **2**, 429–432 (2012).
12. Koenig, S. J., DeConto, R. M. & Pollard, D. Impact of reduced Arctic sea ice on Greenland ice sheet variability in a warmer than present climate. *Geophys. Res. Lett.* **41**, 3933–3942 (2014).
13. Aschwanden, A. et al. Contribution of the Greenland Ice Sheet to sea level over the next millennium. *Sci. Adv.* **5**, eaav9396 (2019).
14. Sinclair, G. et al. Diachronous retreat of the Greenland ice sheet during the last deglaciation. *Quat. Sci. Rev.* **145**, 243–258 (2016).
15. Tarasov, L. & Richard Peltier, W. Greenland glacial history and local geodynamic consequences. *Geophys. J. Int.* **150**, 198–229 (2002).
16. Simpson, M. J. R., Milne, G. A., Huybrechts, P. & Long, A. J. Calibrating a glaciological model of the Greenland ice sheet from the Last Glacial Maximum to present-day using field observations of relative sea level and ice extent. *Quat. Sci. Rev.* **28**, 1631–1657 (2009).
17. Lecavalier, B. S. et al. A model of Greenland ice sheet deglaciation constrained by observations of relative sea level and ice extent. *Quat. Sci. Rev.* **102**, 54–84 (2014).
18. Briner, J. P. et al. Holocene climate change in Arctic Canada and Greenland. *Quat. Sci. Rev.* **147**, 340–364 (2016).
19. Buizert, C. et al. Greenland-wide seasonal temperatures during the last deglaciation. *Geophys. Res. Lett.* **45**, 1905–1914 (2018).
20. Nielsen, L. T., Aðalgeirsdóttir, Gu., Gkinis, V., Nuterman, R. & Hvidberg, C. S. The effect of a Holocene climatic optimum on the evolution of the Greenland ice sheet during the last 10 kyr. *J. Glaciol.* **64**, 477–488 (2018).
21. Larour, E., Seroussi, H., Morlighem, M. & Rignot, E. Continental scale, high order, high spatial resolution, ice sheet modeling using the Ice Sheet System Model (ISSM). *J. Geophys. Res. Earth Surf.* **117**, F01022 (2012).
22. Cuzzone, J. K., Morlighem, M., Larour, E., Schlegel, N. & Seroussi, H. Implementation of higher-order vertical finite elements in ISSM v4.13 for improved ice sheet flow modeling over paleoclimate timescales. *Geosci. Model Dev.* **11**, 1683–1694 (2018).
23. Cuzzone, J. K. et al. The impact of model resolution on the simulated Holocene retreat of the southwestern Greenland ice sheet using the Ice Sheet System Model (ISSM). *Cryosphere* **13**, 879–893 (2019).
24. Downs, J. et al. Western Greenland ice sheet retreat history reveals elevated precipitation during the Holocene thermal maximum. *Cryosphere* **14**, 1121–1137 (2020).
25. Åkesson, H., Nisancioglu, K. H. & Morlighem, M. Simulating the evolution of Hardangerjøkulen ice cap in southern Norway since the mid-Holocene and its sensitivity to climate change. *Cryosphere* **11**, 281–302 (2017).
26. Rignot, E. & Mouginot, J. Ice flow in Greenland for the International Polar Year 2008–2009. *Geophys. Res. Lett.* **39**, L11501 (2012).
27. Morlighem, M. et al. Modeling of Store Gletscher's calving dynamics, West Greenland, in response to ocean thermal forcing. *Geophys. Res. Lett.* **43**, 2659–2666 (2016).
28. .Weidick, A. Observations on some Holocene glacier fluctuations in West Greenland. *Medd. Gronl.* **165** (1968).
29. Larsen, N. K. et al. Rapid early Holocene ice retreat in West Greenland. *Quat. Sci. Rev.* **92**, 310–323 (2014).
30. Lecavalier, B. S. et al. High Arctic Holocene temperature record from the Agassiz ice cap and Greenland ice sheet evolution. *Proc. Natl Acad. Sci. USA* **114**, 5952–5957 (2017).
31. Pendleton, S., Miller, G., Lifton, N. & Young, N. Cryosphere response resolves conflicting evidence for the timing of peak Holocene warmth on Baffin Island, Arctic Canada. *Quat. Sci. Rev.* **216**, 107–115 (2019).
32. McKay, N. P., Kaufman, D. S., Routson, C. C., Erb, M. P. & Zander, P. D. The onset and rate of Holocene neoglacial cooling in the arctic. *Geophys. Res. Lett.* **45**, 12,487–12,496 (2018).
33. Solignac, S., Giraudeau, J. & de Vernal, A. Holocene sea surface conditions in the western North Atlantic: spatial and temporal heterogeneities. *Paleoceanography* **21**, PA2004 (2006).
34. Gibb, O. T., Steinhauer, S., Fréchette, B., de Vernal, A. & Hillaire-Marcel, C. Diachronous evolution of sea surface conditions in the Labrador Sea and Baffin Bay since the last deglaciation. *Holocene* **25**, 1882–1897 (2015).
35. Box, J. E. Greenland Ice Sheet mass balance reconstruction. Part II: surface mass balance (1840–2010). *J. Clim.* **26**, 6974–6989 (2013).
36. Goelzer, H. et al. The future sea-level contribution of the Greenland ice sheet: a multi-model ensemble study of ISMIP6. *Cryosphere Discuss.* https://doi.org/10.5194/tc-2019-319 (2020).
37. Morlighem, M. et al. BedMachine v3: complete bed topography and ocean bathymetry mapping of Greenland from multi-beam echo sounding combined with mass conservation. *Geophys. Res. Lett.* **44**, 11051–11061 (2017).

Methods

Ice-sheet model

To simulate WSW GIS history, we use ISSM v4.13, a finite-element, thermomechanical ice-sheet model[21]. The ice model simulations follow a similar approach to one described previously[22]. For all ice model simulations, we use a higher-order approximation[38,39] to solve the momentum-balance equations. The model domain for this study is similar to a previous regional ice model[23], but is extended to cover the central–west and southwest drainage basins (WSW GIS, Fig. 1). The domain extends from the present-day coastline, where geologic observations show that ice resided at the end of the Younger Dryas[3], eastward to the GIS divide. The northern and southern boundaries of the model domain are located along zones of minimal north-to-south across-boundary flow, on the basis of present-day ice surface velocities[26]. The model uses anisotropic mesh adaptation to produce a non-uniform mesh that varies on the basis of variations in bedrock topography. The bedrock topography is from BedMachine v3[37]. When modelling the WSW GIS during the Holocene, high mesh resolution is necessary[23] in areas of complex bed topography, to prevent artificial ice-margin variability resulting from interaction with bedrock artefacts that occur at coarser resolution. As a result, we construct a mesh that varies from 20-km resolution in areas where gradients in the bedrock topography are smooth, to 2-km resolution in areas where bedrock relief is high.

We use an enthalpy formulation[40] to simulate the thermal evolution of the ice, and geothermal flux[41]. To reduce the computational load associated with using a high number of vertical layers, the model contains only five vertical layers, with the vertical spacing between layers decreasing towards the base. Following ref. [23], we use quadratic finite elements (P1 × P2) along the z axis for the vertical interpolation, which allows the ice-sheet model to capture sharp thermal gradients near the bed, while reducing computational costs associated with running a linear vertical interpolation with increased vertical layers[22].

A spatially varying friction coefficient (k) is derived using inverse methods[21,42], and provides the best match between modelled and interferometric synthetic aperture radar (InSAR) surface velocities[26]: $\tau_b = -k^2 N v_b$, where τ_b represents the basal stress, N represents the effective pressure and v_b is the magnitude of the basal velocity. Using this method, we are able to compute the friction coefficient only under the present-day ice sheet. Across contemporary ice-free areas, a spatially varying drag coefficient is constructed to be proportional to the bedrock elevation[43]: $k = 100 \times \min[\max(0, z_b + 800), z_b]/\max(z_b)$, where z_b is the height of the bedrock. In this case, the friction coefficient remains lower in fjord regions and higher over areas of high topographic relief. We tested the sensitivity of the simulated Holocene ice-mass changes to the choice of the friction coefficient in the contemporary ice-free areas (Methods section 'Sensitivity experiments'). The basal drag coefficient derived using the inverse techniques and scalings described above are allowed to vary through time, following ref. [23]. Here, the basal friction coefficient varies through time on the basis of changes in the simulated basal temperature, ultimately allowing for a time-varying basal friction coefficient. As simulated basal temperatures warm with respect to the present day, the basal friction coefficient decreases (for example, more sliding); as the simulated basal temperatures cool with respect to the present day, the basal friction coefficient increases (for example, less sliding). The ice rheology parameter B is temperature-dependent and follows rate factors shown in ref. [44]. Following refs. [22,23], we initialize B by solving for a present-day thermal steady state, and allow this to evolve during the transient simulations.

Although we include a subelement grounding-line migration scheme[45] in these simulations, we do not include calving parameterization, owing to the prohibitive costs associated with running such a scheme in a higher-order ice model run over palaeoclimate timescales. In addition, owing to poor constraints on past oceanic temperatures throughout the Holocene, particularly at depth, we do not include any submarine melting of floating ice.

Holocene climate forcing

We force our Holocene ice-sheet simulations with spatially and temporally complete palaeoclimate reanalyses[2], which were created using a palaeoclimate data assimilation approach—a method that combines proxy data and climate-model simulations. Specifically[2], oxygen-isotope records from eight ice cores are used for the temperature reanalyses, accumulation records (derived from layer thickness) from five ice cores are used for the precipitation reanalyses, and TraCE21ka (the transient climate evolution experiment[46,47]) is used for both the temperature and precipitation reanalyses. The climate model provides information on the statistical relationships between climate and ice-core variables; all temporal information comes only from the ice-core data. The main reanalysis in ref. [2], which is derived from a priori expectations for the optimal parameters, evaluates well against independent proxy records and is in good agreement with previously published palaeoclimate reconstructions. This reanalysis method[2] obtains mean annual values only. To the temperature reanalyses, we add the temporally varying magnitude of the seasonal cycle, as simulated in TraCE21ka, smoothed by a sixth-order low-pass Butterworth filter with a 4,000 yr^{-1} cutoff frequency. We do not add the seasonal cycle to precipitation, as mean-annual values provide sufficient resolution.

To assess the uncertainty in the main reanalysis[2], both the relationship between oxygen isotopes of ice and temperature and the ice-flow parameters used to derive accumulation from annual layer thickness were varied. For this study, we use the main reanalysis from ref. [2] for our 'moderate' temperature and 'moderate' precipitation (Extended Data Table 1). We use their 'high' and 'low' precipitation reanalyses for our corresponding 'high' and 'low' precipitation scenarios (Extended Data Table 1, Extended Data Fig. 1), and their 'S3' and 'S4' temperature reanalyses for our corresponding 'high' and 'low' temperature scenarios (Extended Data Fig. 2). We choose only these S3 and S4 temperature reanalyses (out of four options) to match the number of precipitation reanalyses, and because these have late-glacial temperature anomalies that are colder, which produces the most realistic results for the ice-margin position at the beginning of our ice-sheet model simulations.

Model experiments

Our ice-sheet model simulations are divided into three experiments: Holocene (12,500 years ago to AD 1850), historic (AD 1850–2012) and future (AD 2015–2100). The surface mass balance over the Holocene and historic periods is computed using a positive degree day (PDD) method[48]. Details regarding the climate forcings used in the PDD algorithm to construct the accumulation and ablation history are provided in the subsections below. We use degree-day factors of 4.3 mm $°C^{-1}$ d^{-1} and 8.3 mm $°C^{-1}$ d^{-1} for snow and ice, respectively, with allocation for the formation of superimposed ice[49]. A lapse rate of 6 °C km^{-1} is used to adjust the temperature of the climate forcings to the ice-surface elevation. Further details regarding the PDD algorithm can be found in ref. [50]

Holocene simulations. Our simulations for the Holocene begin 12,500 years ago, when the ice margin across WSW Greenland was at or near the present-day coastline. As input into the PDD algorithm to create the necessary ablation and accumulation history, we rely on the previous reanalysis of temperature and precipitation anomalies[2] (Extended Data Figs. 1, 2), as described above, at 50-year temporal resolution. We use three temperature and precipitation reconstructions, with the timing and amplitude of changes during the Holocene varying between the reconstructions (Extended Data Table 1). The reanalysis anomalies are from the AD 1850–2000 mean, with the precipitation anomaly being expressed as a fraction of the mean AD 1850–2000 precipitation. Temperature and precipitation spanning the Holocene are given as $T_t = \underline{T}_{(1850–2000)} + \Delta T_t$ and $P_t = \underline{P}_{(1850–2000)} \Delta P_t$, where $\underline{T}_{(1850–2000)}$ and $\underline{P}_{(1850–2000)}$ represent the monthly mean temperature and precipitation for the period AD 1850–2000 from ref. [35], and ΔT_t and ΔP_t represent the monthly anomalies. Our choice of

applying anomalies to a higher-resolution climatology follows traditional methodology for forcing ice-sheet models back through time. We account for uncertainty in the response of the ice-sheet model to temperature and precipitation reconstructions by creating an ensemble of nine individual ISSM simulations that have varying temperature and precipitation forcings (Figs. 2, 3, Extended Data Table 1), which is possible owing to the independence of the temperature and precipitation reconstructions[2].

Holocene simulation boundary conditions. At the southern, northern and ice-divide boundaries we impose Dirichlet boundary conditions. Flux at the ice front is unconstrained. The boundary conditions come from a GIS spin-up performed over one glacial cycle (beginning 125,000 years ago). For the climate forcing, we use a method whereby the AD 1850–2000-mean surface air temperature and precipitation[35] is scaled back through time on the basis of isotopic variations in the Greenland Ice Core Project (GRIP) $\delta^{18}O$ record[51]. From this, we create the transient boundary conditions of ice thickness, ice temperature and ice velocities. The use of these simplified climate boundary conditions for the full ice-sheet spin-up is justified because the ice divides in the continental GIS simulation do not undergo major shifts during the Holocene, and so there are minimal changes in the across-boundary fluxes. Furthermore, running the nine separate continental-scale GIS simulations over the Holocene would be computationally prohibitive. Each of the regional simulations therefore use the same boundary conditions, and differences between each simulation are the result of the different climate forcings used.

We initialize the regional ice-sheet model using present-day ice-surface elevation from a Greenland Ice Mapping Project digital elevation model[52], and let the model relax for 20,000 years to the applied 12,500-years-ago climate until ice volume and basal temperatures equilibrate. This time is chosen as the starting point of our simulations, as the ice margin over WSW Greenland was near or at the present-day coastline and the margin was relatively stable during this interval[53]. The model is forced transiently through time from 12,500 years ago to AD 1850 using the climatologies discussed in Methods subsection 'Holocene simulations'. We use an adaptive timestep, which varies between 0.02 and 0.1 years, depending on the Courant–Friedrichs–Lewy criterion[54], with linear interpolation between timesteps. A time-dependent forcing[55] that accounts for relative sea-level changes is applied, which affects the area available for glaciation and the presence of floating ice.

Historic simulations. To simulate the ice history up to the year AD 2012, we construct the surface mass balance using existing monthly temperature and precipitation fields[35]. We initialize the historic simulations with each individual Holocene model (nine simulations). Although the individual Holocene simulations differ with respect to the ice geometry and volume at AD 1850, the simulated rates of mass change from AD 1850 to AD 2012 remain similar (Fig. 3), and capture trends and features associated with reconstructions of ice mass change from ref. [35].

Future simulations. To calculate the future mass-rate changes across WSW Greenland (Fig. 3), we performed continental GIS-scale simulations, which are part of the Ice Sheet Model Intercomparison Project for CMIP6 (ISMIP6)[56]. Our future comparisons for the mass change of WSW Greenland come directly from these continental-scale GIS simulations. We extract ice-mass changes for our WSW domain from these continental simulations to compare with the ice-mass loss simulated by our regional model over the Holocene and historic periods.

The continental model is initialized in a similar manner to the regional model (see Methods section 'Ice-sheet model'). The model uses a higher-order ice-flow approximation[3,4], is extruded to five layers, and uses higher-order vertical finite elements[10] to compute the thermal evolution of the ice sheet. The horizontal mesh resolution varies from 3 km where there is high relief in the bedrock topography to 20 km in the ice-sheet interior. The initial friction coefficient is modified through time on the basis of variations in the simulated basal temperature[2]. The model is spun up over one glacial cycle (beginning 125,000 years ago) using a method whereby the AD 1850–2000-mean surface air temperature and precipitation[20] is scaled back through time on the basis of isotopic variations in the GRIP $\delta^{18}O$ record. We use a PDD model[15] to derive the surface mass balance through time (degree-day factors: snow, 4.3 mm $°C^{-1}$ d^{-1}; ice, 8.3 mm $°C^{-1}$ d^{-1}).

During the glacial–interglacial spin-up, the ice front is located at the present-day bedrock–ocean margin. From AD 1840 to AD 1979, the model spin-up continues, but uses the surface mass balance from ref. [35]. In AD 1970, the ice front is imposed to be at the present-day ice margin (any area where the simulated ice margin at AD 1970 is outside the present-day ice margin is set to present-day). Between AD 1979 and AD 2014, the RACMO2.3[57] surface mass balance anomalies from the AD 1979–1989 mean is applied to the climatology from ref. [35] (AD 1979–1989 mean minus the AD 1850–1900 mean).

ISSM has a free-flux condition at all ice margins. Beginning in AD 2015, these simulations are forced up to AD 2100 following the ISMIP6 protocol[56,58]. The ISMIP6 forcings consist of yearly surface mass balance and oceanic retreat derived from CMIP5 and CMIP6 climate output[28], for selected future climate scenarios (CMIP5 RCP2.6 and RCP8.5, CMIP6 SSP126 and SSP585). For these simulations, we chose to use only the surface mass balance forcings (atmosphere only), to be consistent with our Holocene simulations, which did not include any calving parameterization. Our simulations correspond to tier-1 and tier-2 ISMIP6 Greenland simulations[28]. To make comparisons among a range of ice-sheet models, all using different initialization and spin-up procedures, the control run is removed in other representations of our future simulations, particularly for the purpose of ISMIP6[36]. However, we chose to not remove the control run from our simulated future ice-mass changes (Figs. 3, 4). Because our palaeoclimate ice-sheet simulations do not have a control run and our simulated future changes probably include dynamic memory of past ice changes reflected in our palaeoclimate spin-up, the comparison between our simulated past, present and future ice-mass changes are consistent.

Sensitivity experiments. We run two experiments to test the sensitivity of the simulated Holocene ice-mass changes to model parameters: sensitivity to the choice of the friction coefficient in contemporary ice-free areas, and sensitivity to our reference climatology. Our first method to calculate the friction coefficient is described above (Methods section 'Ice-sheet model'). The second method uses a natural neighbour interpolation to extrapolate the friction coefficient calculated from the inversion under the present-day ice extent to beyond the present-day ice extent. Extended Data Fig. 3 shows the difference in the friction coefficient between the model using a friction coefficient derived as a function of bedrock topography and a model using a friction coefficient derived by extrapolation. The difference is zero over present-day ice-covered areas, as both methods use a friction coefficient derived from an inversion.

In Extended Data Fig. 4, the simulated ice-mass changes over the Holocene are shown for a simulation using the basal friction coefficients determined by extrapolation and the basal friction coefficient derived as proportional to the bedrock topography. Both of these simulations use the climate forcings of simulation 1 (Extended Data Table 1). Although the friction coefficient derived on the basis of the bedrock topography is larger in most regions outside the present-day ice margin, this has little effect on the simulated mass changes.

We also simulated ice-mass change across our domain for two runs using temperature and precipitation forcings of simulation 7 (Extended Data Table 1). We use two different mean time periods (the reference time from ref. [2], AD 1850–1950 mean, and AD 1850–2000 mean) as the reference climatology[35] to which the temperature and precipitation anomalies from ref. [2] are applied. This test was performed because the ice-core proxies that were used in the data assimilation framework contain little information past around AD 1970. The experiment shows minimal impact on trends in Holocene ice-mass change between the two reference periods (Extended Data Fig. 5).

Data–model comparison

To assess the performance of the model simulations against geologic data, we compared the simulated ice margins from each model run ($n = 9$) with reconstructed GIS margins[3] The reconstructed ice margins represent five discrete time intervals during which the GIS halted its overall pattern of retreat to deposit extensive moraine systems throughout the domain, although the most detailed portion of the moraine record exists in the northern part of our model domain[3]. When considering the entire domain, our simulations exhibit good agreement with independent observations (Extended Data Fig. 6). We quantify the comparison in the northern domain, where the palaeo-ice margins are well mapped[3] (Fig. 1, Extended Data Fig. 7), the moraine chronology is most secure[4] (Fig. 2), and the ice marginal setting is dominated by large tracts of land-based ice with few fjords[23], reducing the influence of ice dynamics on ice-margin change and enhancing the influence on surface mass balance control of ice-margin change. To conduct this data–model comparison in the northern domain, we calculated areas for the reconstructed and simulated ice sheets 11,600, 10,400, 9,100, 8,100 and 7,300 years ago, with an eastern boundary at the ice divide, and northern and southern boundaries shown in Extended Data Fig. 7. We then calculated the percentage difference in ice-sheet area between the reconstruction and each model simulation. We found that simulated ice areas are −19% to +4% the size of ice areas constrained by observations (moraines), suggesting generally good agreement between the model and observations (Extended Data Table 2).

Data availability

Original data published here are ice-sheet model output (Gt per century and Gt per year) and modified palaeoclimate data from ref. [2], which are available at https://www.ncdc.noaa.gov/paleo/study/30172. The simulations we performed made use of the open-source ISSM and are available at https://issm.jpl.nasa.gov/ (last access 1 July 2019)[21].

38. Blatter, H. Velocity and stress fields in grounded glaciers: a simple algorithm for including deviatoric stress gradients. *J. Glaciol.* **41**, 333–344 (1995).
39. Pattyn, F. A new three-dimensional higher-order thermomechanical ice sheet model: Basic sensitivity, ice stream development, and ice flow across subglacial lakes. *J. Geophys. Res. Solid Earth* **108**, 2382 (2003).
40. Aschwanden, A., Bueler, E., Khroulev, C. & Blatter, H. An enthalpy formulation for glaciers and ice sheets. *J. Glaciol.* **58**, 441–457 (2012).
41. Shapiro, N. M. & Ritzwoller, M. H. Inferring surface heat flux distributions guided by a global seismic model: particular application to Antarctica. *Earth Planet. Sci. Lett.* **223**, 213–224 (2004).
42. Morlighem, M. et al. Spatial patterns of basal drag inferred using control methods from a full-Stokes and simpler models for Pine Island Glacier, West Antarctica. *Geophys. Res. Lett.* **37**, L14502 (2010).
43. Åkesson, H., Morlighem, M., Nisancioglu, K. H., Svendsen, J. I. & Mangerud, J. Atmosphere-driven ice sheet mass loss paced by topography: Insights from modelling the south-western Scandinavian Ice Sheet. *Quat. Sci. Rev.* **195**, 32–47 (2018).
44. Cuffey, K. M. & Paterson, W. S. B. *The Physics of Glaciers* (Academic Press, 2010).
45. Seroussi, H. et al. Dependence of century-scale projections of the Greenland ice sheet on its thermal regime. *J. Glaciol.* **59**, 1024–1034 (2013).
46. Liu, Z. et al. Transient simulation of last deglaciation with a new mechanism for Bølling-Allerød warming. *Science* **325**, 310–314 (2009).
47. He, F. et al. Northern Hemisphere forcing of Southern Hemisphere climate during the last deglaciation. *Nature* **494**, 81–85 (2013).
48. Tarasov, L. & Peltier, W. R. Impact of thermomechanical ice sheet coupling on a model of the 100 kyr ice age cycle. *J. Geophys. Res. Atmos.* **104**, 9517–9545 (1999).
49. Janssens, I. & Huybrechts, P. The treatment of meltwater retention in mass-balance parameterizations of the Greenland ice sheet. *Ann. Glaciol.* **31**, 133–140 (2000).
50. Le Morzadec, K., Tarasov, L., Morlighem, M. & Seroussi, H. A new sub-grid surface mass balance and flux model for continental-scale ice sheet modelling: testing and last glacial cycle. *Geosci. Model Dev.* **8**, 3199–3213 (2015).
51. Dansgaard, W. et al. Evidence for general instability of past climate from a 250-kyr ice-core record. *Nature* **364**, 218–220 (1993).
52. Howat, I. M., Negrete, A. & Smith, B. E. The Greenland Ice Mapping Project (GIMP) land classification and surface elevation data sets. *Cryosphere* **8**, 1509–1518 (2014).
53. Young, N. E. & Briner, J. P. Holocene evolution of the western Greenland Ice Sheet: Assessing geophysical ice-sheet models with geological reconstructions of ice-margin change. *Quat. Sci. Rev.* **114**, 1–17 (2015).
54. Courant, R., Friedrichs, K. & Lewy, H. Über die partiellen Differenzengleichungen der mathematischen Physik. *Math. Ann.* **100**, 32–74 (1928).
55. Caron, L. et al. GIA model statistics for GRACE hydrology, cryosphere, and ocean science. *Geophys. Res. Lett.* **45**, 2203–2212 (2018).
56. Nowicki, S. M. J. et al. Ice Sheet Model Intercomparison Project (ISMIP6) contribution to CMIP6. *Geosci. Model Dev.* **9**, 4521–4545 (2016).
57. Noël, B. et al. Evaluation of the updated regional climate model RACMO2.3: summer snowfall impact on the Greenland Ice Sheet. *Cryosphere* **9**, 1831–1844 (2015).
58. Nowicki, S. et al. Experimental protocol for sea level projections from ISMIP6 standalone ice sheet models. *Cryosphere Discuss*. https://doi.org/10.5194/tc-2019-322 (2020).

Acknowledgements We acknowledge field logistical support by CH2MHill Polar Field Services. We acknowledge support by NSF-Arctic System Sciences grants ARC-1504267 to J.P.B., B.C. and E.K.T., ARC-1503281 to E.J.S. and G.J.H., ARC-1504230 to M.M., ARC-1503959 to N.E.Y. and J.M.S., and ARC-1504457 to J.V.J.; and NSF-Earth Sciences Instrumentation and Facilities grant 1652274 to E.K.T. J.A.B. acknowledges NSF Graduate Research Fellowship (DGE-1256082); A.A.C. acknowledges NSF Graduate Research Fellowship (DGE-1645677). A.d.V. and E.A. acknowledge support from the Natural Sciences and Engineering Council of Canada (NSERC) and the Fonds de Recherche du Québec - Nature et Technologie (FRQNT). S.N. acknowledge support from the NASA Sea Level Change Team and Cryosphere Sciences Programs. J.M.S. acknowledges support by the Unger Vetlesen Foundation and the Columbia Climate Center. This is LDEO contribution number 8436.

Author contributions The project was conceived by J.P.B., N.E.Y., J.M.S., E.K.T., B.C., E.J.S., G.J.H., M.M., E.L. and J.V.J. J.P.B., J.K.C., J.A.B. and E.J.S. wrote the first draft of the manuscript. All authors commented on and edited the manuscript. N.E.Y., E.K.T. and J.P.B. led the fieldwork, with contributions from O.B., A.A.C., A.J.L., J.K.C. and J.A.B. J.K.C. led ice-sheet modelling with N.-J.S., E.L., M.M., J.V.J. and J.D. J.A.B. led climate forcing with E.J.S. and G.J.H. A.J.L., J.K.C. and J.P.B. carried out the data–model comparison. A.d.V. and E.A. provided information on sea-surface conditions. S.N. led ISMIP6 climate forcing used in this study.

Competing interests The authors declare no competing interests.

Additional information

Supplementary information is available for this paper at https://doi.org/10.1038/s41586-020-2742-6.

Correspondence and requests for materials should be addressed to J.P.B.

Peer review information *Nature* thanks Andy Aschwanden and the other, anonymous, reviewer(s) for their contribution to the peer review of this work.

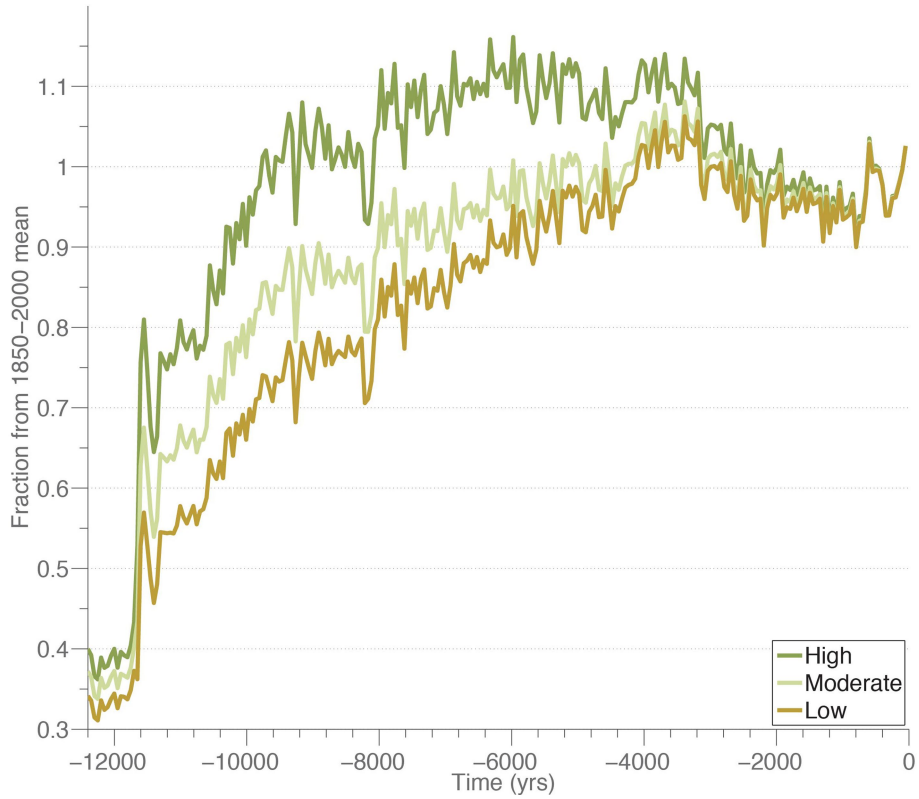

Extended Data Fig. 1 | Precipitation forcing for the Holocene ice-sheet simulation. The area-averaged (over model domain) mean annual precipitation is shown for three different reconstructions[2].

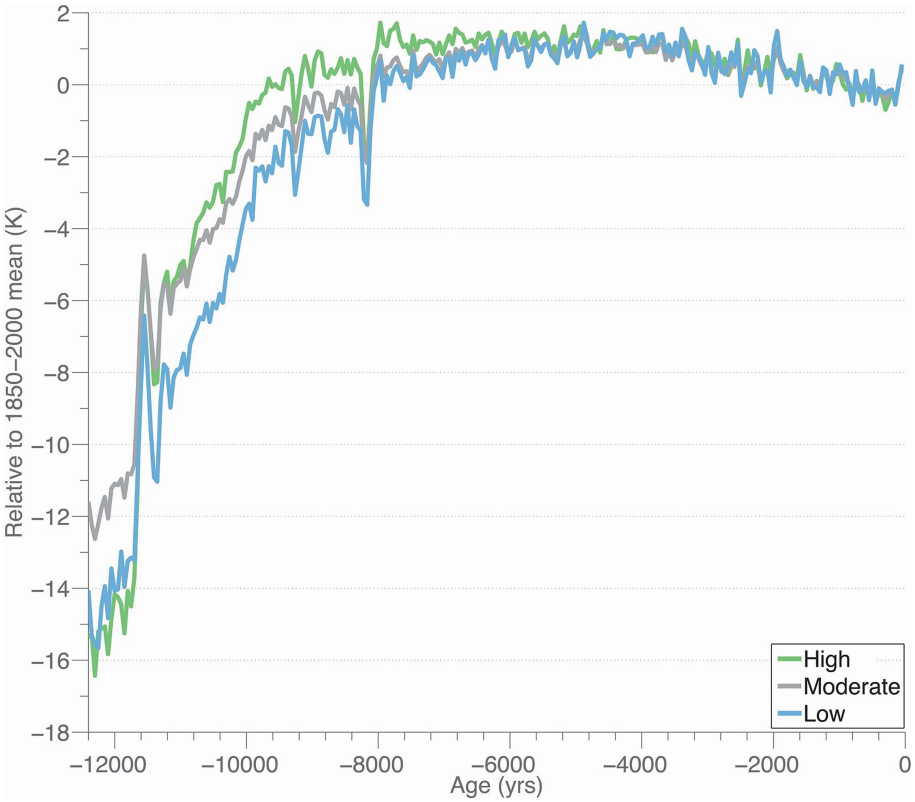

Extended Data Fig. 2 | Temperature forcing for the Holocene ice-sheet simulation. The area-averaged (over model domain) mean annual temperature is shown for three different reconstructions[2].

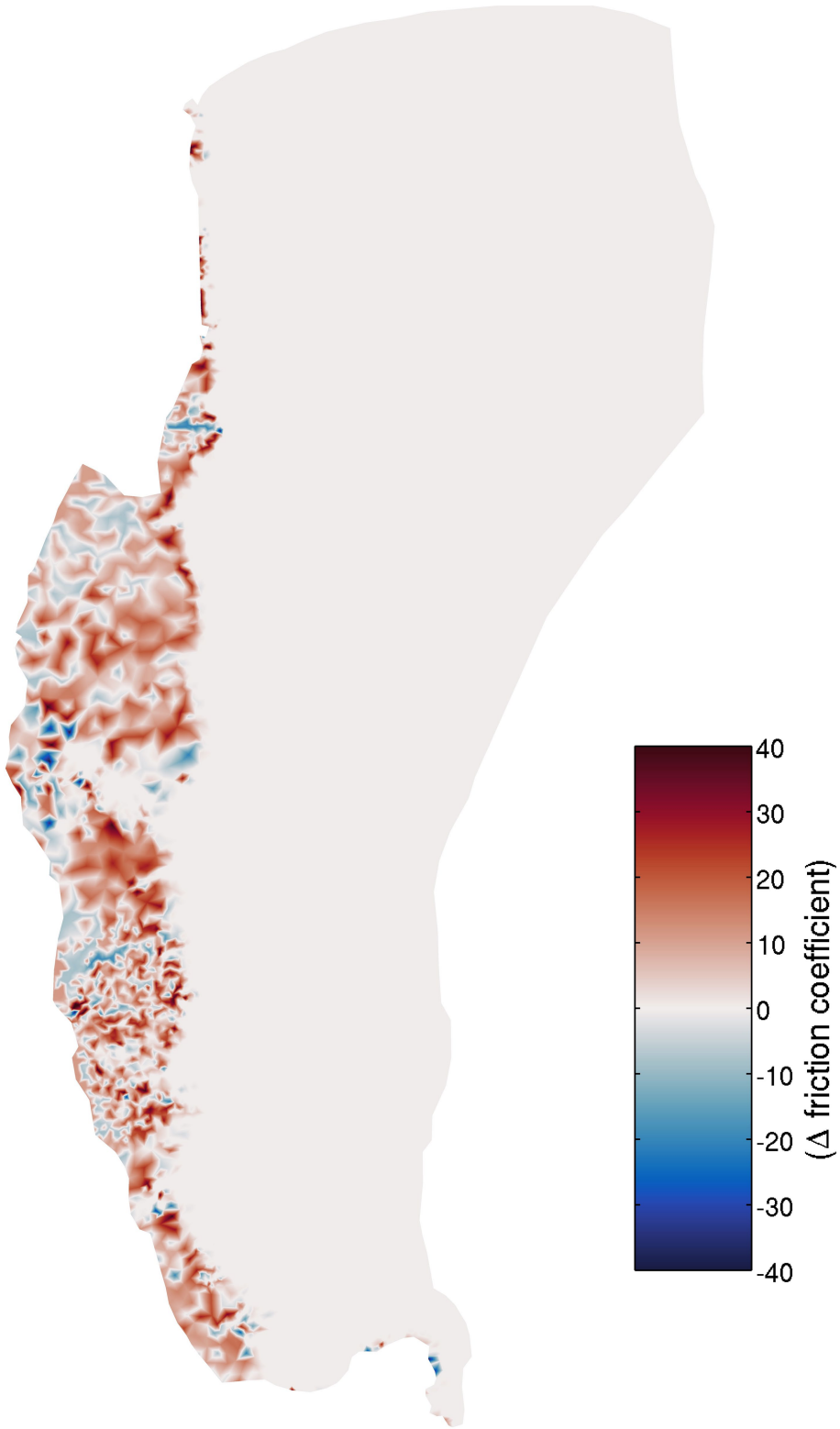

Extended Data Fig. 3 | Basal-friction sensitivity experiment. The map shows the difference in the friction coefficient between the model using a friction coefficient proportional to the bedrock topography and a model using a friction coefficient derived by extrapolation. Red shows where the friction coefficient proportional to the bedrock topography is higher than the friction coefficient derived from extrapolation.

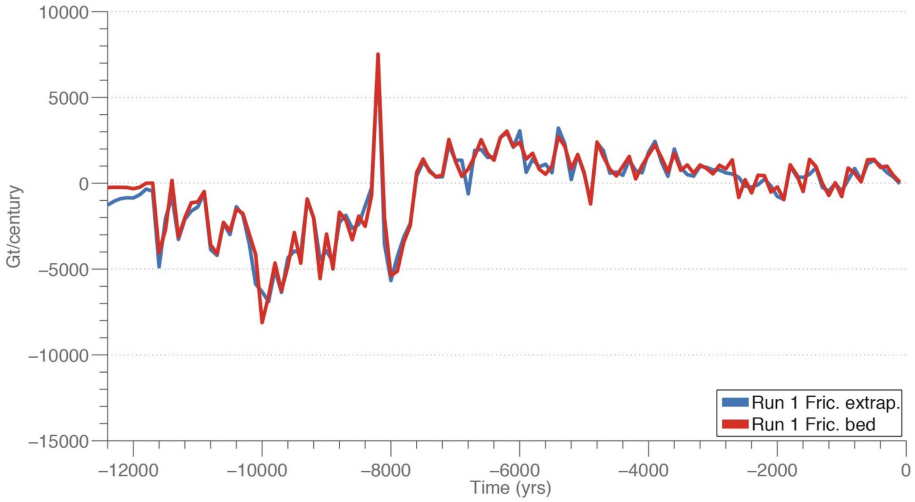

Extended Data Fig. 4 | Sensitivity experiment showing the influence of basal friction on simulated GIS mass change. The simulated ice-mass change (Gt per century) in the Holocene is shown using climatologies from model run 1 (Extended Data Table 1), with reference friction coefficients outside the present-day ice margin derived as a function of the bed topography (red) or as an extrapolation of friction coefficients (blue).

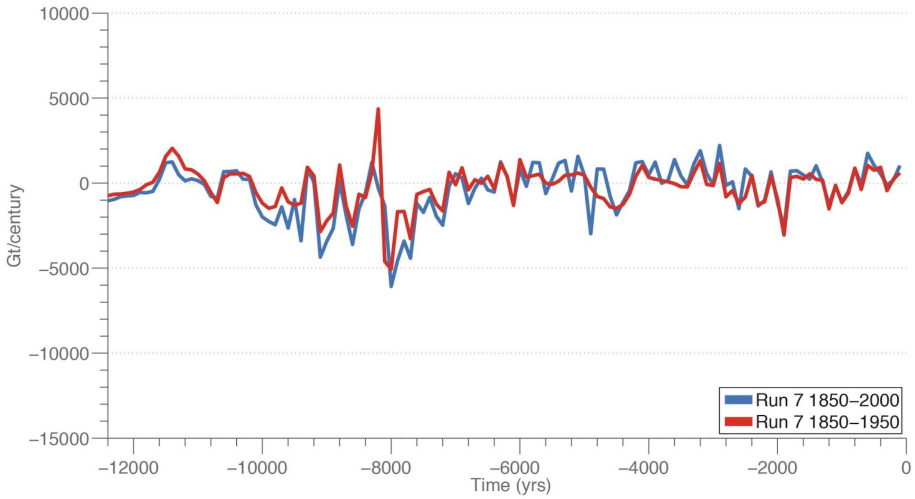

Extended Data Fig. 5 | Climatology sensitivity experiment. The simulated ice-mass change (Gt per century) in the Holocene is shown using two different reference climatologies (monthly mean) of temperature and precipitation from ref. [35], to which the temperature and precipitation anomalies from ref. [2] are applied. Blue, simulated ice-mass change using the AD 1850–2000-mean reference climatology (the same reference period as in ref. [2]); red, simulated ice-mass change using the AD 1850–1950-mean reference climatology. The climate anomalies[2] applied to the reference climatologies are the same as for model run 7 (Extended Data Table 1).

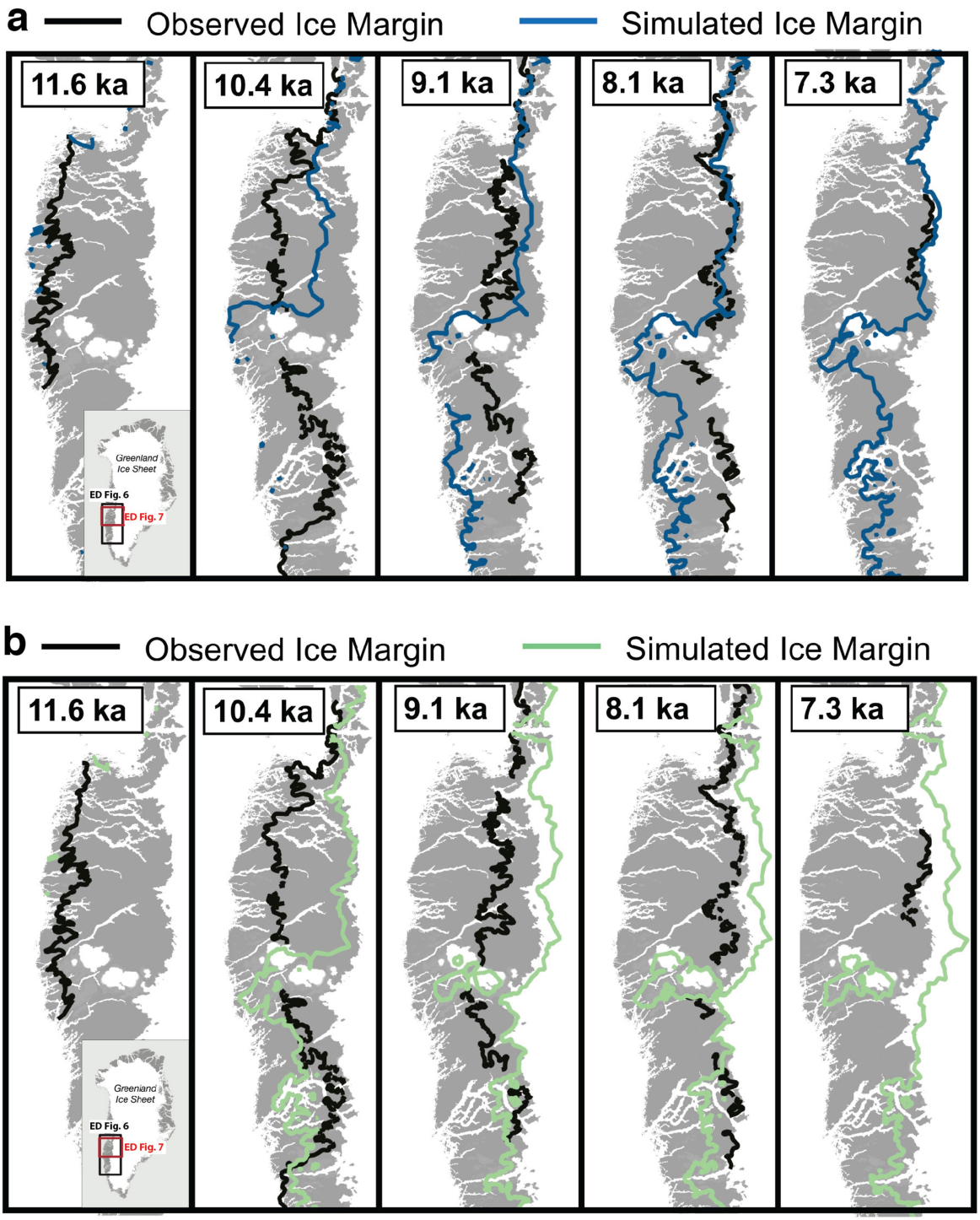

Extended Data Fig. 6 | Data–model comparison of ice-margin change. **a**, Maps showing the simulated (blue) and observed (black; from geologic reconstruction) ice margin for model simulation 7. **b**, Maps showing the simulated (green) and observed (black; from geologic reconstruction) ice margin for model simulation 1. See Extended Data Table 1 for a description of the model simulations. ka, thousand years ago.

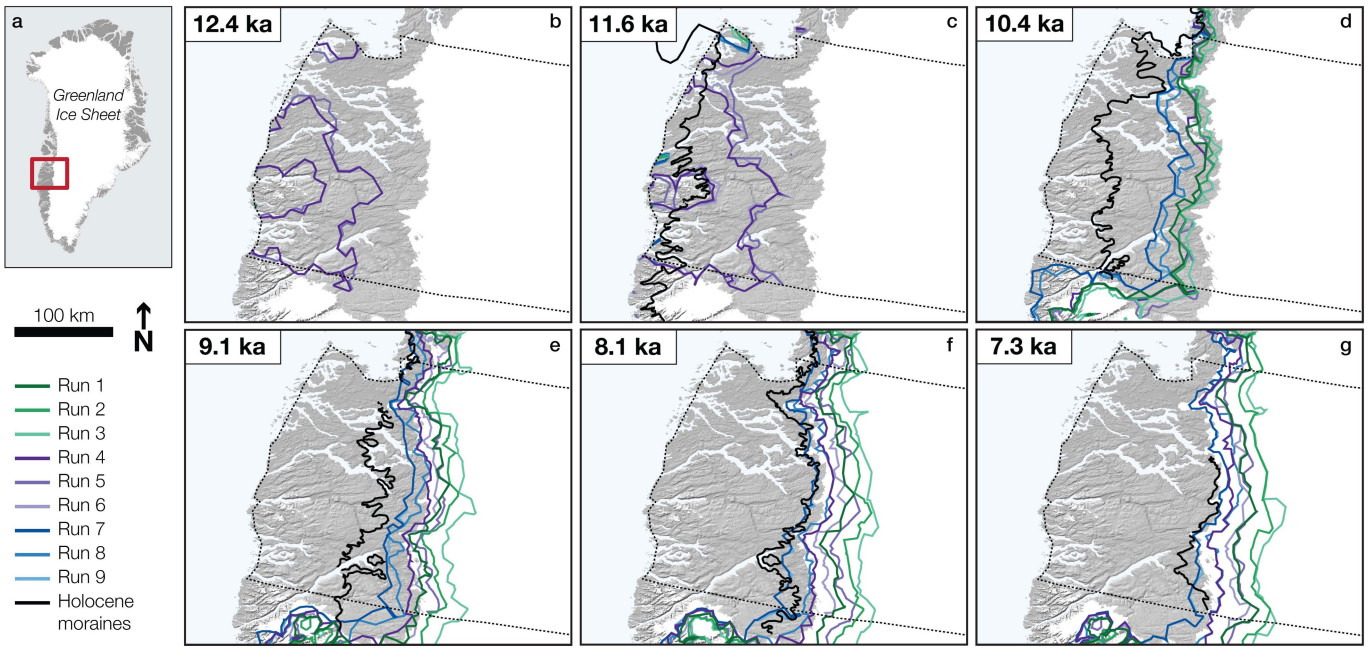

Extended Data Fig. 7 | Goodness-of-fit exercise in the area with detailed moraine records. a–g, Comparison of modelled and reconstructed ice margins in the northern domain (**a**) at six different time slices (**b**–**g**). Field-reconstructed ice margins[3] are represented by the black lines. Simulated ice margins not shown in **b** are at the domain boundary or coastline; some margins in **d** lie beneath other margins, making them invisible; dashed lines demarcate the comparison domain.

Extended Data Table 1 | Holocene ice-sheet model simulations and the corresponding temperature and precipitation combinations

Model Run	Temperature Scenario	Precipitaton Scenario
1	High	High
2	High	Moderate
3	High	Low
4	Moderate	High
5	Moderate	Moderate
6	Moderate	Low
7	Low	High
8	Low	Moderate
9	Low	Low

Extended Data Table 2 | Data–model fit in the northern domain

	Model run								
Margin age (ka)	1	2	3	4	5	6	7	8	9
12.4	0%	0%	0%	-12%	-12%	-12%	0%	0%	0%
11.6	4%	4%	4%	-10%	-18%	-13%	4%	4%	4%
10.4	-16%	-17%	-18%	-16%	-16%	-17%	-11%	-12%	-11%
9.1	-15%	-18%	-19%	-11%	-13%	-16%	-7%	-9%	-7%
8.1	-11%	-16%	-19%	-7%	-10%	-13%	-1%	-6%	-1%
7.3	-11%	-16%	-17%	-6%	-9%	-11%	-1%	-6%	-2%

For each time slice, we calculated the percentage difference between the area enclosed by the reconstructed ice margin and the area enclosed by the modelled ice margin. Positive values indicate areas where the modelled area is larger than the reconstructed area; negative values indicate that the modelled area is smaller than the reconstructed area.